Temporal Structure Mining for Weakly Supervised Action Detection

Tan Yu[1]*, Zhou Ren[2]*, Yuncheng Li[3], Enxu Yan[3], Ning Xu[4]* and Junsong Yuan[5]
[1] Cognitive Computing Lab, Baidu Research [2] Wormpex AI Research
[3] Snap Inc. [4] Amazon [5] State University of New York at Buffalo
v_yutan@baidu.com, renzhou200622@gmail.com, raingomm@gmail.com,
eyan2@snap.com, ningxu01@gmail.com, jsyuan@buffalo.edu

Abstract

Different from the fully-supervised action detection problem that is dependent on expensive frame-level annotations, weakly supervised action detection (WSAD) only needs video-level annotations, making it more practical for real-world applications. Existing WSAD methods detect action instances by scoring each video segment (a stack of frames) individually. Most of them fail to model the temporal relations among video segments and cannot effectively characterize action instances possessing latent temporal structure. To alleviate this problem in WSAD, we propose the temporal structure mining (TSM) approach. In TSM, each action instance is modeled as a multi-phase process and phase evolving within an action instance, i.e.*, the temporal structure, is exploited. In this framework, phase filters are used to calculate the confidence scores of the presence of an action's phases in each segment. Since in the WSAD task, frame-level annotations are not available and thus phase filters cannot be trained directly. To tackle the challenge, we treat each segment's phase as a hidden variable. We use segments' confidence scores from each phase filter to construct a table and determine hidden variables, i.e., phases of segments, by a maximal circulant path discovery along the table. Experiments conducted on three benchmark datasets demonstrate good performance of the proposed TSM.*

1. Introduction

Thanks to the video representation learned by deep neural network, the community has achieved excellent performance in action recognition task on trimmed video clips [30, 35, 41, 5, 38, 37]. Nevertheless, people are usually interested in action instances occurring in short intervals of a video. Therefore, directly applying the classifier trained by trimmed videos in untrimmed videos usually leads to failure. In order to alleviate the above problem, research community turns to the action detection task [9, 15, 3, 43, 19, 7], which is to temporally localize action instances and meanwhile recognize their categories. Recently, substantial success has been achieved in fully-supervised action detection [36, 10, 12, 43, 19, 7], which relies on precise frame-level action labels. Nevertheless, in a large-scale application, labelling frame-level annotations is too costly.

*This work was done when the authors were at Snap Inc.

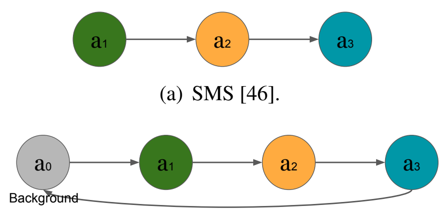

(a) SMS [46].

(b) The proposed TSM.

Figure 1. Comparisons between SMS [46] and the proposed TSM. In SMS, the phase evolves in start(a_1)-middle(a_2)-end(a_3) order and thus it can only model a single action instance. In contrast, the proposed TSM additionally introduces a background phase, a_0. The phase evolves in a recurrent order, which is simple but effectively models the videos contains multiple action instances.

To relieve the demand for frame-level annotations, weakly supervised action detection methods are proposed recently [40, 21]. These methods only require video-level labels, which indicates the presence of certain action instances. Compared with frame-level annotations, video-level labels are easier to obtain. UntrimmedNets [40] partitions a video into overlapped sliding windows, and the detection is conducted by selecting sliding windows with high salient scores. More recently, STPN [21] decomposes a video into multiple short video segments of a uniform size and learns to select a subset of segments. Nevertheless, both UntrimmedNets and STPN score segments individually and ignore the relation among them in action instances. Observing the limitations of existing methods, we are motivated to exploit the temporal relations among segments.

Temporal relations have been extensively exploited in the fully-supervised action detection. Representative works include RNN-based approach [16], 3D-convolution approach [23] and temporal pyramid pooling [47]. Nevertheless, these methods are not applicable to weakly-supervised

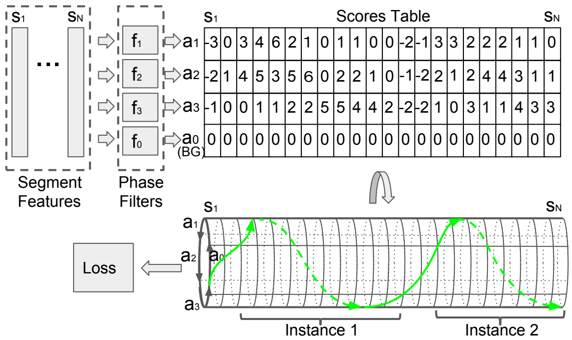

Figure 2. An untrimmed video V is partitioned into multiple video segments $\{s_i\}_{i=1}^{N}$. Each segment s_i is fed into backbone network to obtain its feature. Each action is factorized into M phase $\{a_m\}_{m=1}^{M}$ ($M = 3$ in this case). Additionally, a background (BG) phase a_0 is devised. M action phase filters $\{f_m\}_{m=1}^{M}$ as well as a background phase filter f_0 take segments' features as input and obtain confidence scores of each segment for each phase. Action detection is converted into a maximal circulant path discovery problem in the confidence score table. In the training stage, the score of the discovered maximal path is used for computing the classification loss to learn phase-wise filters and update the backbone network. In the testing stage, action instances are consecutive sequences of segments separated by the background phase.

scenarios since we have no knowledge of when an action instance starts and finishes. On the other hand, the start-middle-end structure designed by SMS [46] does not work well either since it can only model a single instance. Due to this limitation, each training sample of SMS contains only a single action instance trimmed by the provided frame-level labels, which are not available in the weakly-supervised scenario. How to exploit temporal structure in an unsupervised scenario remains an unsolved problem.

In this work, we model each action instance as a multi-phase process like SMS [46] and SSN [47]. But we introduce an additional background phase to model the background which separates multiple action instances in an untrimmed video. It is simple but effectively address the action detection in videos containing multiple action instances. In Figure 1, we visualize the phase evolving as well as the phase evolving in SMS [46]. In SMS, the phase evolves in a start(a_0)-middle (a_1)-end(a_2) order. Therefore, it is only able to model a single action instance. In contrast, ours evolves in a recurrent order and effectively models videos containing multiple action instances. We define the pattern of the phase evolving as **temporal structure**. We utilize phase filters to describe confidence score of the presence of each phase on each segment. Since in weakly-supervised settings, we have no knowledge of when an action instance starts or finishes, therefore, phase filters cannot be trained directly as SSN [47]. To tackle this challenge, we treat the phase of each segment as a hidden variable. After obtaining the table of phase-wise confidence scores, phases of segments are determined through maximal circulant path discovery, which is efficiently solved through dynamic programming. In the training stage, the score of the discovered maximal path constructs the classification loss to learn phase filters and update the backbone network. In the testing stage, detected action instances are consecutive sequences of segments in non-background phases.

An interesting observation is that the maximal path discovery on the phase-wise confidence score table relies on the output of phase filters, while the optimization of filters' weights depends on classification loss computed by the discovered maximal path. Their mutually dependent relation leads us to adopt an alternately updating strategy. We alternately discover the maximal path based on current phase filters and update phase filters using gradient derived from the classification loss of the discovered maximal path. Figure 2 visualizes the architecture of the proposed temporal structure mining (TSM) approach. As shown in the figure, an untrimmed video is partitioned in multiple segments, and the segments' features are obtained from the backbone network. Phase filters take the segment-level features as input to generate phase-wise confidence scores table. The action detection is formulated into finding a maximal circulant path in the scores table, while the score of the maximal path is used to compute classification loss. The gradient is derived based on the loss to update TSM. Extensive experiments on three public datasets show that our TSM considerably outperforms state-of-the-art methods.

2. Related Work

Weakly-supervised action detection. Inspired by the success of weakly supervised learning in object detection [1], UntrimmedNets [40] formulates weakly supervised action detection task as a multiple instance learning problem. It learns attention weights on cropped video sliding window or proposals. Similarly, STPN [21] selects the key segments by imposing a sparsity constraint on the learned attention. More recently, Auto-Loc [29] utilizes Outer-Inner-Contrastive to obtain a more reliable boundary. Nevertheless, UntrimmedNet, STPN and Auto-Loc are based on per-segment class activation and the temporal structure among a video's segments are ignored. Different from previous methods, we seek to exploit the temporal structure inherited in the action to improve the action detection performance.

Temporal structure. Context-Free Grammar (CFG) [26] decomposes a human activity into multiple sub-events and manually design an action grammar. Actom Sequence Model (ASM) [11] models actions as sequences of actoms. It manually annotates actoms for a set of training actions. Nevertheless, the manual annotations used in both CFG and ASM are subjective to annotators and might cost huge amount of labors for a large dataset. Similarly, attributes used in [18] and concepts used in [32] are also manually defined. Tang *et al.* [34] partitions a video into a series of events and designs a variable-duration hidden Markov model (HMM) to model the events transitions. But the huge amount of parameters of the designed HMM makes the training difficult. Wang *et al.* [39] decompose an action into atoms and phases. Clustering is used to discover action atoms and continuous atoms are merged into AND/OR structure phases. Nevertheless, it does not consider the case when a video contains uninterested background. It might be only applicable for action recognition on trimmed videos. Structured Segment Network (SSN) [47] divides an action instance into three stages and utilizes temporal pyramid pooling to explicitly exploit temporal structure. Since in the fully-supervised scenario, the start and end of an action instance are known in training dataset, it is straightforward to construct the temporal pyramid. Nevertheless, in the weakly-supervised cases, no temporal annotations are provided, and thus we are not able to conduct temporal pyramid pooling used in SSN. Structural Maximal Sum (SMS) [46] also exploits the temporal structure in action instances. SMS designs a start-middle-end structure, which can only model a single action instance. In the training phase, due to single instance limitation, SMS has to manually crop a whole video into clips containing a single action instance using the provided temporal annotations. Nevertheless, in weakly-supervised scenarios, no temporal annotations are provided, making the training of SMS infeasible. Meanwhile, some methods [2, 6, 25] align videos to transcripts. They rely on temporal orderings of manually defined basic actions. In contrast, ours only relies on video-level class label and automatically discovers the action phases.

3. Problem Formulation

3.1. Definition

Given a video V, we uniformly decompose it into N short video segments $[s_1, \cdots, s_N]$. For each action class c, we define M action phases $\{a_j\}_{j=1}^M$ and model each action instance as a M-phase process. Meanwhile, the background is modelled by phase a_0. We define $\mathbf{x}_i = g(s_i, \mathbf{W})$ as the feature of segment s_i obtained from backbone where $\mathbf{W}$ contains parameters of backbone. $v_{c,i}^j$ is defined as the confidence score of the presence of phase a_j of class c in s_i:

$$v_{c,i}^j = f(\mathbf{x}_i, \mathbf{w}_c^j, b_c^j) = \mathbf{x}_i^\top \mathbf{w}_c^j + b_c^j, \tag{1}$$

where $f(\cdot, \mathbf{w}_c^j, b_c^j)$ represents j-th action phase filter for the class c. We use $v_{c,i}^j$ to construct the confidence score table visualized in Figure 3 where $v_{c,i}^j$ is filled in the cell located in row j and column i. We define (i, p_i) as the cell in the score table where the column index i is the segment index, and the row index p_i is the phase index, where $p_i \in [0, M]$. We define $[(1, p_1), \cdots, (N, p_N)]$ as a path in the confidence score table. For convenience, we omit the column index and represent a path of class c by $\mathcal{P}_c = [p_1, \cdots, p_N]$.

3.2. Temporal Structure Mining

Now we describe the phase evolving constraint, which is the core component of temporal structure modelling. Given a segment s_i in the phase p_i, the phase p_{i+1} of its next segment s_{i+1} only has two choices: 1) remaining the same phase as s_i, 2) evolving to the next phase. Formally,

$$p_{i+1} \in \{p_i, (p_i + 1)\%(M + 1)\}. \tag{2}$$

The mod operation $\%$ means that the last phase a_M evolves to the background phase a_0 and a_0 evolves to the first action phase a_1. In other words, the action phase transits in a circulant manner. This recurrent evolving mechanism effectively handles videos containing multiple action instances.

Given an untrimmed video V, we obtain phase-wise confidence scores of each segment $\{v_{c,i}^j\}_{j=1}^M$ through Eq. (1) to construct the confidence score table. Given a path $\mathcal{P}_c = [p_1, p_2, \cdots, p_N]$, we define the path score $F_c(\mathcal{P}_c)$ as

$$F_c(\mathcal{P}_c) = \sum_{i=1}^N \mathbb{1}(p_i \neq 0) v_{c,i}^{p_i}. \tag{3}$$

where $\mathbb{1}(p_i \neq 0)$ is the indicator function omitting segments in background phase. Since the background's scores are not used in computing path score, by setting the background score $v_{c,i}^0 = 0$, we obtain an equivalent but simpler form as

$$F_c(\mathcal{P}_c) = \sum_{i=1}^N v_{c,i}^{p_i}. \tag{4}$$

The temporal structure mining is formulated into discovering a path constrained by Eq. (2) with maximal path score:

$$\mathcal{P}_c^* = \underset{\mathcal{P}_c}{\operatorname{argmax}} F_c(\mathcal{P}_c). \tag{5}$$

We show an example of maximal circulant path in Figure 3 by green boxes. In the training stage, the score of maximal circulant path $F_c(\mathcal{P}_c^*)$ represents the presence of action c in the video, which constructs the classification loss. In the testing stage, the action instances of a certain class are detected by grouping consecutive segments separated by background phase. As shown in Figure 3, it detects two action instances, which are separated by background.

Until now, two problems remain unsolved: 1) how to learn phase filters $\{f(\cdot, \mathbf{w}_c^j, b_c^j)\}_{j=1}^M$ in Eq. (1); 2) how to discover the maximal circulant path $\mathcal{P}_c^*$ in Eq. (5) efficiently. In Section 3.3 and 3.4, we tackle them, respectively.

3.3. Phase Filter Learning

Without frame-level action annotations, learning phase filters is much more difficult than its fully-supervised counterpart [47, 46]. We observe that filters learning relies on the discovered maximal path, and on the same time the maximal path discovery depends on pre-trained phase filters.

a_1	-1.3	-2.0	0.3	0.4	0.6	0.2	0.1	0.1	0.0	-0.1	-0.5	0.3	0.2	0.2	0.1	-0.3
a_2	-2.1	-3.1	0.4	0.5	0.3	0.5	0.6	0.2	0.1	-0.2	-0.7	0.1	0.2	0.6	0.2	-0.2
a_3	-3.1	0.8	-0.3	0.1	0.1	0.2	0.2	0.5	0.2	-0.2	-0.3	-0.3	0.3	0.1	0.4	-0.3
a_0 (BG)	0.0	0.0	0.0	0.0	0.0	0.0	0.0	0.0	0.0	0.0	0.0	0.0	0.0	0.0	0.0	0.0
			Instance 1									Instance 2				

Figure 3. An example for confidence score table. The green bold cells are along the maximal circulant path. Due to the phase evolving constraint, maximal path discovery is not equivalent to greedily selecting the phase with highest score for each segment. For instance, in the second column of the table, we select phase a_0, the background phase (background), even though phase a_3 has the largest confidence score in this column.

Algorithm 1 Alternately Updating

Input: Videos $\{V_k\}_{k=1}^K$ and ground-truth labels $\{\mathbf{y}_k\}_{k=1}^K$.
Output: Weights of the phase filters $\{\mathbf{w}_c^j, b_c^j\}_{j=1,c=1}^{M,C}$, backbone network weights $\mathbf{W}$.

for $c = 1$ to C **do**
  for $j = 1$ to M **do**
    initialize $\mathbf{w}_c^j$,b_c^j
for $k = 1$ to K **do**
  $V_k \to [s_{k,1}, \cdots, s_{k,N}]$
for $t = 1$ to T **do**
  for $k = 1$ to K **do**
    $\mathbf{x}_{k,i} \leftarrow g(s_{k,i}, \mathbf{W})$
    for $c = 1$ to C **do**
      discover $\mathcal{P}_{k,c}^*$ based on Algorithm 2
      compute $\mathcal{L}_c$ based on Eq. (6)
      for $j = 1$ to M **do**
        compute $\frac{\partial \mathcal{L}_c}{\partial \mathbf{w}_c^j}$ and $\frac{\partial \mathcal{L}_c}{\partial b_c^j}$ based on Eq. (7)
        $\mathbf{w}_c^j \leftarrow \mathbf{w}_c^j - \delta \frac{\partial \mathcal{L}_c}{\partial \mathbf{w}_c^j}$, $b_c^j \leftarrow b_c^j - \delta \frac{\partial \mathcal{L}_c}{\partial b_c^j}$
      for $i = 1$ to N **do**
        compute $\frac{\partial \mathcal{L}_c}{\partial \mathbf{x}_{k,i}}$ based on Eq. (8)
    compute $\frac{\partial \mathcal{L}_c}{\partial \mathbf{W}}$ use Eq. (9)
    $\mathbf{W} \leftarrow \mathbf{W} - \delta \frac{\partial \mathcal{L}_c}{\partial \mathbf{W}}$
return $\{\mathbf{w}_c^j\}_{j=1,c=1}^{M,C}$, $\mathbf{W}$.

Their mutually dependence leads to the fact that the training process can not be conducted in a sequential manner.

To tackle this problem, we adopt an alternately updating strategy consisting of two steps. In the first step, the maximal path $\mathcal{P}_c^*$ is discovered based on output of currently phase filters $\{f(\cdot, \mathbf{w}_c^j, b_c^j)\}_{j=1}^M$, using Maximal Path Discovery as discussed in Sec. 3.4 (Algorithm 2). In the second step, the path score of detected maximal path $F_c(\mathcal{P}_c^*)$ and the video's ground-truth class label $y_c \in \{0, 1\}$ are used to compute the classification loss $\mathcal{L}_c$ defined as

$$\begin{aligned} \mathcal{L}_c = & - y_c \log(\tanh(F_c(\mathcal{P}_c^*) + \epsilon) \\ & - (1 - y_c) \log(1 - \tanh(F_c(\mathcal{P}_c^*)). \end{aligned} \tag{6}$$

Note that, $\mathcal{L}_c$ is not the standard cross-entropy loss. We replace $\mathrm{sigmoid}(\cdot)$ used in original cross-entropy loss by $\tanh(\cdot)$. Below we explain the reason. By setting all the segments in background phase, we can obtain a trivial path $\hat{\mathcal{P}}_c = [0, 0, \cdots, 0]$. Since $F_c(\hat{\mathcal{P}}_c) = 0$, the maximal path's score $F_c(\mathcal{P}_c^*) \in [0, +\infty]$. It means that $\mathrm{sigmoid}(F_c(\mathcal{P}_c^*)) \in [1/2, 1)$ and thus the standard cross-entropy loss is no longer feasible. Therefore, we use $\tanh(\cdot)$ to replace $\mathrm{sigmoid}(\cdot)$ since $\tanh(F_c(\mathcal{P}_c^*)) \in [0, 1)$. ϵ is a small positive value to ensure $\tanh(F_c(\mathcal{P}_c^*) + \epsilon) > 0$.

Based on the loss function defined above, the gradients of loss with respect to weights of phase filters and the backbone are derived through back-propagation as Eq. (7)(9). We alternately discover maximal path and update weights in each iteration until the maximal iteration is reached. Algorithm 1 describes the training procedure.

$$\begin{aligned} \frac{\partial \mathcal{L}_c}{\partial \mathbf{w}_c^j} &= \frac{\partial \mathcal{L}_c}{\partial F_c(\mathcal{P}_{k,c}^*)} \sum_{i=1}^N \mathbb{1}(p_i = j) \frac{\partial v_{i,c}^j}{\partial \mathbf{w}_c^{p_i}}, \\ \frac{\partial \mathcal{L}_c}{\partial b_c^j} &= \frac{\partial \mathcal{L}_c}{\partial F_c(\mathcal{P}_{k,c}^*)} \sum_{i=1}^N \mathbb{1}(p_i = j) \frac{\partial v_{i,c}^j}{\partial b_c^{p_i}}. \end{aligned} \tag{7}$$

$$\frac{\partial \mathcal{L}_c}{\partial \mathbf{x}_{k,i}} = \frac{\partial \mathcal{L}_c}{\partial F_c(\mathcal{P}_{k,c}^*)} \sum_{j=1}^M \mathbb{1}(p_i = j) \frac{\partial v_{i,c}^j}{\partial \mathbf{x}_{k,i}}. \tag{8}$$

$$\frac{\partial \mathcal{L}_c}{\partial \mathrm{vec}(\mathbf{W})} = \sum_{i=1}^N \left[\frac{\partial \mathbf{x}_{k,i}}{\partial \mathrm{vec}(\mathbf{W})} \right]^\top \frac{\partial \mathcal{L}_c}{\partial \mathbf{x}_{k,i}}, \tag{9}$$

where $\mathrm{vec}(\cdot)$ unfolds $\mathbf{W}$ to a vector. Despite that the proposed algorithm supports backbone weights updating, limited by computing resources, we fix the backbone network in implementation and use it as a feature extraction module.

3.4. Maximal Path Discovery

Naively, $F_c(\mathcal{P}_c^*)$ can be obtained through exhaustively searching over all possible paths satisfying the defined temporal constraint. Nevertheless, the exhaustive search takes $\mathcal{O}(M2^N)$ complexity, making it inscalable with respect to N. Thanks to the temporal constraint in phase transition, the maximal path discovery problem can be tackled efficiently by dynamic programming in $\mathcal{O}(MN)$ complexity.

Recall that, the phases of segments satisfy the temporal constraint defined in Eq. (2). As shown in Figure 4, let us

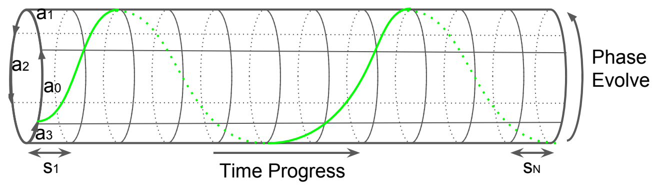

Figure 4. Temporal structure mining is converted into maximal circulant path discovery along cylindrical surface from top surface to bottom surface. The green curve is the maximal circulant path.

represent time progress as step-right operation and represent phase evolves as the step-clockwise operation. Constrained by the temporal consistency, when determining the phase of the next segment, it has two choices: 1) step right, 2) step right and simultaneously step clockwise. The first choice represents the phase of the next segment remains the same as the current segment. On the other hand, the second choice is that an action evolves to another phase in next segment. The circulant phase transition settings makes the problem equivalent to finding a maximal circulant path along the cylindrical surface. Since dynamic programming is based on back tracking, we rewrite Eq. (2) originally for forward tracking into its back-tracking version to facilitate the derivation of dynamic programming:

$$p_{i-1} \in \{(p_i + M)\%(M+1), p_i\}. \tag{10}$$

We define $S^j_{c,i}$ as maximal score of all possible paths starting from segment s_1 and ending in segment s_i with phase j for class c. Based on Eq. (10), it is straightforward to obtain

$$S^j_{c,i} = \max\{S^j_{c,i-1}, S^{j\downarrow}_{c,i-1}\} + v^j_{c,i}, \tag{11}$$

where

$$j\downarrow \;=\; (j+M)\%(M+1). \tag{12}$$

$F_c(\mathcal{P}^*_c)$ can be obtained through

$$F_c(\mathcal{P}^*_c) = \max_{j\in[0,M]} S^j_{c,N}. \tag{13}$$

The procedure of the maximal path discovery is described in Algorithm 2. Since it only has $N \times M$ iterations to obtain $\mathcal{P}^*_c$ and $F_c(\mathcal{P}^*_c)$, the time complexity is only $\mathcal{O}(NM)$.

3.5. Soft-max Path Discovery

Note that, the aforementioned maximal path discovery process only selects the path with the highest score. In this case, the gradient is only back-propagated through cells along the maximal path, leaving cells not in the maximal path ignored. To exploit more information in scores table and stabilizes the training. In this section, we propose a soft-max path discovery algorithm. The idea is simply replacing the Eq. (11) by its soft counterpart:

$$S^j_{c,i} \leftarrow \max{}^{\alpha}(S^j_{c,i-1}, S^{j\downarrow}_{c,i-1}) + v^j_{c,i}, \tag{14}$$

where $\max^{\alpha}(\cdot,\cdot)$ is a soft-max operator defined as:

$$\max{}^{\alpha}(x, y) = \log(e^{\alpha x} + e^{\alpha y})/\alpha, \tag{15}$$

in which α is a positive constant controlling the softness. It is not difficult to observe that

$$\lim_{\alpha\to+\infty} \max{}^{\alpha}(x, y) = \max(x, y). \tag{16}$$

By default we set $\alpha = 10$. In soft-max path discovery,

Algorithm 2 Maximal Path Discovery

Input: The segments features $[\mathbf{x}_1, \cdots, \mathbf{x}_N]$, an action type c and weights of the phase filters $\{\mathbf{w}^j_c, b^j_c\}^M_{j=1}$.
Output: The maximal path $\mathcal{P}^*_c = [p_1, \cdots, p_N]$. The path score of maximal path $F_c(\mathcal{P}^*_c)$.

for $j = 0$ to M **do**
  $v^j_{c,1} \leftarrow \mathbf{x}_1^\top \mathbf{w}^j_c + b^j_c$
  $S^j_{c,1} \leftarrow v^j_{c,1}$
for $i = 2$ to N **do**
  for $j = 0$ to M **do**
    $v^j_{c,i} \leftarrow \mathbf{x}_i^\top \mathbf{w}^j_c + b^j_c$
    if $S^j_{c,i-1} > S^{j\downarrow}_{c,i-1}$ **then**
      $S^j_{c,i} \leftarrow S^j_{c,i-1} + v^j_{c,i},\; P^j_i \leftarrow j$
    else
      $S^j_{c,i} \leftarrow S^{j\downarrow}_{c,i-1} + v^j_{c,i},\; P^j_i \leftarrow j\downarrow$
$F_c(\mathcal{P}^*_c) \leftarrow \max_{j\in[0,M]} S^j_{c,N}$
$p_N \leftarrow \text{argmax}_{j\in[0,M]} S^j_{c,N}$
for $i = N-1$ to 1 **do**
  $p_i \leftarrow P^{p_{i+1}}_{i+1}$
return $\mathcal{P}^*_c$ and $F_c(\mathcal{P}^*_c)$.

$$\bar{F}_c(\mathcal{P}^*_c) = \log(\sum_{j=0}^{M} e^{\alpha S^j_{c,N}})/\alpha. \tag{17}$$

In back-propagation,

$$\frac{\partial \mathcal{L}_c}{\partial \mathbf{w}^j_c} = \frac{\partial \mathcal{L}_c}{\partial \tilde{F}_c(\mathcal{P}^*_c)} \sum_{j=0}^{M} \frac{e^{\alpha S^j_{c,N}}}{\sum_{j'=1}^{N} e^{\alpha S^{j'}_{c,N}}} \frac{\partial S^j_{c,N}}{\partial \mathbf{w}^j_c}. \tag{18}$$

From Eq. (18), we can observe that it counts multiple paths into consideration and assigns different weights according to their importance. Note that, the soft-max path discovery is only conducted in training. In contrast, in testing, we still conduct maximal path discovery to detect action instances. Algorithm 3 describes the soft-max path discovery.

3.6. Relation with existing methods

Structured Segment Network (SSN) [47] also exploits the temporal structure in temporal action detection. They divide each action proposal into starting, course and ending stages. They further obtain an instance's representation through temporal pyramid pooling. Since they deal with a fully-supervised scenario, the positive training proposals are available to perform structured temporal pyramid pooling. Nevertheless, in a weakly-supervised scenario, we do not have access to temporal annotations, making temporal pyramid pooling no longer feasible.

Structural Maximal Sum (SMS) [46] designs a start-middle-end structure for modeling a single action instance.

Algorithm 3 Soft-Max Path Discovery

Input: The segments' features $[\mathbf{x}_1, \cdots, \mathbf{x}_N]$, an action type c and weights of the phase filters $\{\mathbf{w}_c^j, b_c^j\}_{j=1}^M$.
Output: The path score of soft path $\bar{F}_c(\mathcal{P}_c^*)$.

for $j = 0$ to M **do**
  $v_{c,1}^j \leftarrow \mathbf{x}_1^\top \mathbf{w}_c^j + b_c^j$
  $S_{c,1}^j \leftarrow v_{c,1}^j$
for $i = 2$ to N **do**
  for $j = 0$ to M **do**
    $v_{c,i}^j \leftarrow \mathbf{x}_i^\top \mathbf{w}_c^j + b_c^j$
    $S_{c,i}^j \leftarrow \max^\alpha(S_{c,i-1}^j, S_{c,i-1}^{j\downarrow}) + v_{c,i}^j$
$\bar{F}_c(\mathcal{P}_c^*) \leftarrow \log(\sum_{j=0}^M e^{\alpha S_{c,N}^j})/\alpha$
return $\bar{F}_c(\mathcal{P}_c^*)$.

SMS is also designed for fully-supervised action detection. Utilizing the known ground-truth action instances' boundaries, they partition a video into several positive training samples containing a single action instance. Nevertheless, in a weakly supervised scenario, an untrimmed video might contain multiple instances. In that case, an action instance might start after the finish of another action instance and thus the start-middle-end structure designed for a single action instance does not work well.

4. Experiments

In this section, we first describe the benchmark datasets, evaluation metrics, backbone network and implementation details. After that, we conduct ablation study to analyze the contribution of individual modules and then compare the proposed TSM with state-of-the-art techniques.

4.1. Datasets and Evaluation Metrics

We evaluate TSM on three popular action localization benchmark datasets, THUMOS14 [14], ActivityNet 1.2 [4] and ActivityNet 1.3 [4]. Videos on both datasets are untrimmed and we do not utilize the temporal boundary annotations in the training stage. On THUMOS14 dataset, we train our model with the 20-class validation subset, which consists of 200 untrimmed videos, without using the temporal annotations. Following the settings in [21], we evaluate our algorithm using the 212 videos in the 20-class testing subset with temporal annotations. ActivityNet 1.2 consists of $4,819$ training videos and $2,383$ videos for validation, covering 100 activity classes. ActivityNet 1.3 consists of $10,024$ videos for training, $4,926$ for validation, with 200 activity classes. On ActivityNet 1.2 and ActivityNet 1.3 datasets, we use training split as the training set and test on the validation set. We follow the standard evaluation protocol based on mean average precision values at several different levels of intersection over union (IoU) thresholds. All datasets are evaluated by the standard action detection evaluation programs provided by the datasets.

4.2. Backbone Network and Two-stream Fusion

Since compared baselines adopt different features, to make a fair comparison with baselines, we adopt two types of backbone networks to extract features for video segments. The first backbone is I3D [5] pretrained on the Kinetics dataset [17], which are also adopted by one of our compared baseline STPN [21]. The second backbone is TSN [41] pretrained by UntrimmedNet [40], which is also used by one of our compared baseline Auto-Loc [28]. Even though our algorithm supports an end-to-end training as derived in Eq. (9), due to limited computing resources, we only use backbone as feature extraction modules.

It is demonstrated in many previous methods [21] that, by fusing multiple information such as RGB and optical flow achieves a considerably better performance than using a single modality. Therefore, we utilize two separate networks which takes RGB and optical flow as input, respectively. The detection results from two-stream networks are further fused to obtain the final detection results. To be specific, given a video V and a specific class type c, we first obtain the candidate temporal intervals $\mathcal{I}_{rgb} = \{I_{rgb}^i\}_{i=1}^{K_{rgb}}$ and $\mathcal{I}_{of} = \{I_{of}^i\}_{i=1}^{K_{of}}$ based on a single RGB or optical-flow (of) network, respectively. The final score of each interval $I \in \mathcal{I}_{rgb} \cup \mathcal{I}_{of}$ is obtained by combining its score from the RGB network and that from the optical-flow network

$$F_c(I) = \frac{F_c^{rgb}(I) + \lambda F_c^{of}(I)}{1 + \lambda}. \tag{19}$$

We set $\lambda = 2$ on the THUMOS14 dataset and set $\lambda = 0.5$ on ActivityNet 1.2 and ActivityNet 1.3 datasets. Since there exist overlapping intervals in $\mathcal{I}_{rgb} \cup \mathcal{I}_{of}$, we conduct non-maximal suppression on intervals based on their scores.

4.3. Implementation Details

For the RGB stream, we rescale the smallest dimension of a frame to 256 and perform the center crop of size 224×224. For the flow stream, we apply the TV-L1 optical flow algorithm [42]. Pixel values of obtained optical flows are truncated to the range $[-20, 20]$, then rescaled between -1 and 1. We sample 400 segments at uniform interval from each video. The network is trained using traditional SGD optimizer. The learning rate is initialized as 0.005 and decays to its $\frac{1}{10}$ every 10 epochs. The whole training process stops at 30 epochs and the performance is considerably stable with respect to weights initialization. At testing time, for each class, we rank detected candidate locations according to their structural scores.

	2-phase					3-phase				
mAP@IoU	0.3	0.4	0.5	0.6	0.7	0.3	0.4	0.5	0.6	0.7
RGB	29.5	22.1	15.1	7.3	2.7	30.8	22.7	15.5	7.6	3.4
Optical Flow	36.1	29.3	22.9	13.6	**6.9**	37.1	30.4	23.4	13.3	7.0
Two-stream	**39.3**	**31.7**	**24.6**	**14.1**	6.6	**39.5**	**31.9**	**24.5**	**13.8**	**7.1**

Table 1. Two-stream fusion on THUMOS14 dataset.

	2-phase					3-phase				
mAP@IoU	0.5	0.6	0.7	0.8	0.9	0.5	0.6	0.7	0.8	0.9
RGB	28.0	24.0	19.4	14.7	8.4	28.1	23.8	19.5	14.7	8.2
Optical Fow	22.5	19.6	16.5	12.9	7.0	23.1	20.3	17.4	13.2	7.7
Two-stream	**29.7**	**25.6**	**20.8**	**15.8**	**9.0**	**30.3**	**25.7**	**21.4**	**16.1**	**9.0**

Table 2. Two-stream fusion on ActivityNet 1.3 dataset.

M	mAP@IoU					
	0.3	0.4	0.5	0.6	0.7	Avg
1	37.1	29.7	22.7	12.6	6.1	21.6
2	39.3	31.7	**24.6**	**14.1**	6.6	23.3
3	**39.5**	**31.9**	24.5	13.8	**7.1**	**23.4**
4	38.9	31.0	23.8	13.2	6.5	22.7
5	38.2	30.6	23.5	13.0	6.3	22.3

Table 3. Influence of M on the THUMOS14 dataset.

4.4. Ablation Study

Influence of phase number. We evaluate the influence of phase number M on THUMOS14 dataset. We use I3D features. We vary the phase number M among $[1, 5]$. Note that, when phase number is 1, it is equivalent to selecting foreground from background and ignoring the temporal structure. As shown in Table 3, the performance significantly improves when M increases from 1 to $\{2, 3\}$, which validates the superiority of exploiting the temporal structure. Meanwhile, the performance turns worse when M further increases to $\{4, 5\}$. The worse performance might be due to the fact that 3 phases are enough to model the temporal structure of most action instances in THUMOS14 dataset and more phases are more prone to over-fitting.

Soft-max Path Discovery. We demonstrate the advantage of soft-max path discovery over its counterpart based on maximal path discovery. The experiments are conducted on THUMOS14 dataset based on two-stream I3D features with 2-phase settings. As shown in Table 4, the soft-max path discovery converges faster than its counterpart. It only need 30 epochs whereas its hard counterpart requires 45 epochs. Meanwhile, the performance of soft-max path discovery consistently outperforms its hard counterpart. For instance, when IoU $= 0.3$, the mAP achieved by soft path discovery is 39.3, whereas its hard counterpart only achieves a 38.7 mAP. Moreover,

Two-stream fusion. We show the performance improvement through fusing the RGB stream and the optical-flow stream on THUMOS14 and ActivityNet 1.3 datasets. The results are obtained from I3D segment features. As shown in Table 1 and Table 2 , fusing the detection results from two streams generally achieves better action detection performance than that based on a single modality. One exception is the case when IoU $= 0.7$ on THUMOS14 dataset at a 2-phase setting. In that case, using a single RGB stream

Supervision	Epochs	mAP@IoU		
		0.3	0.5	0.7
Hard	45	38.7	24.0	6.2
Soft	30	**39.3**	**24.6**	**6.6**

Table 4. The comparison between soft-max path discovery (Soft) and maximal path discovery (Hard) on THUMOS14 dataset.

Supervision	Method	mAP@IoU		
		0.3	0.5	0.7
Full	Richard *et al.* [24]	30.0	15.2	–
Full	Yeung *et al.* [44]	36.0	17.1	–
Full	Yuan *et al.* [45]	33.6	18.8	–
Full	Yuan *et al.* [46]	36.5	17.8	–
Full	S-CNN [29]	36.3	19.0	5.3
Full	CDC [27]	40.1	23.3	7.9
Full	Dai *et al.* [8]	–	25.6	9.0
Full	SSAD [19]	43.0	24.6	–
Full	R-C3D [43]	44.7	28.9	–
Full	SS-TAD [3]	45.7	29.2	9.6
Full	Gao *et al.* [13]	50.1	31.0	9.9
Full	SSN [47]	51.9	29.8	10.7
Weak	Sun *et al.* [33]	8.5	4.4	–
Weak	Hide and Seek [31]	19.5	6.8	–
Weak	UntrimmedNets [40]	31.1	16.2	5.1
Weak	STPN [21]	35.5	16.9	4.3
Weak	Auto-Loc [28]	35.8	21.2	5.8
Weak	W-TLAC [22]	**40.1**	22.8	**7.6**
Weak	Our (TSN)	37.3	21.9	6.0
Weak	Our (I3D)	39.5	**24.5**	7.1

Table 5. Comparisons with state-of-the-art methods under different IoU thresholds on THUMOS14 dataset.

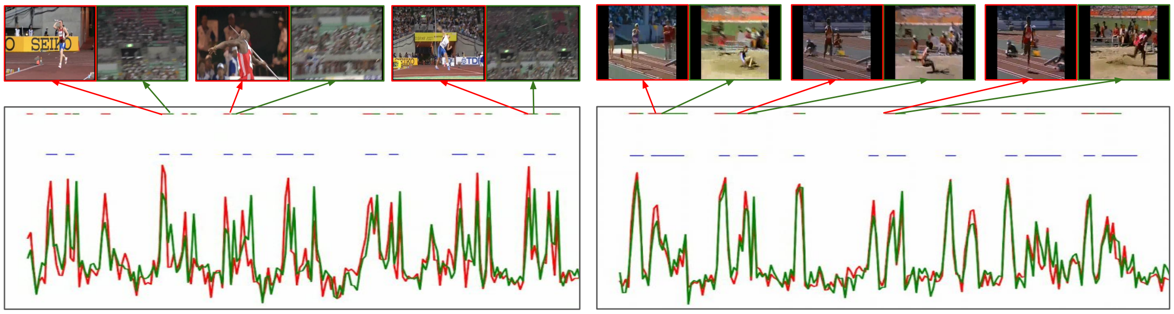

(a) 'JavelinThrow' action detection on video_test_0001159. (b) 'LongJump' action detection on video_test_0000379

Figure 5. Green curves are the activations of phase-1 filter and red curves are activations of phase-2 filter. Blue lines are ground-truth locations of action instances. Green lines are locations of segments in phase 1 and red lines are locations of segments in phase 2.

Supervision	Method	mAP@IoU									
		0.5	0.55	0.6	0.65	0.7	0.75	0.8	0.85	0.9	0.95
Full	SSN [47]	41.3	38.8	35.9	32.9	30.4	27.0	22.2	18.2	13.2	6.1
Weak	UntrimmedNets [40]	7.4	6.1	5.2	4.5	3.9	3.2	2.5	1.8	1.2	0.7
Weak	Auto-Loc [28]	27.3	24.9	22.5	19.9	17.5	15.1	13.0	10.0	6.8	3.3
Weak	TSM (Ours)	**28.3**	**26.0**	**23.6**	**21.2**	**18.9**	**17.0**	**14.0**	**11.1**	**7.5**	**3.5**

Table 6. Comparisons with the state-of-the-art methods under different IoU thresholds on ActivityNet 1.2 dataset.

Supervision	Method	mAP@IoU		
		0.5	0.75	0.95
Full	Montes *et al.* [20]	22.5	–	–
Full	R-C3D [43]	26.8	–	–
Full	CDC [27]	45.3	26.0	0.2
Full	SSN [47]	43.3	28.7	5.6
Weak	STPN [21]	29.3	16.9	2.3
Weak	TSM (Ours)	**30.3**	**19.0**	**4.5**

Table 7. Comparisons with the state-of-the-art methods under different IoU thresholds on ActivityNet 1.3 dataset.

achieves a 6.9 mAP whereas the two-stream only achieves a 6.6 mAP. The worse performance might be due to the fact that the performance of the optical-flow stream is much worse than that of the RGB-stream.

4.5. Comparison with state-of-the-art methods

To further demonstrate the effectiveness of our method, we compare it with current state-of-art methods on THUMOS14, AcitivityNet 1.2 and AcitivityNet 1.3 datasets. To make a fair comparison with Auto-Loc [29] on ActivityNet 1.2, we adopt the same TSN features released by the authors of Auto-Loc. Meanwhile, to fairly compare with STPN [21] on ActivityNet 1.3, we use the same I3D features. Moreover, we show our results using both TSN and I3D features on THUMOS14 dataset. We compare ours with both fully-supervised action detection methods and weakly supervised ones. As shown in Table 5 6 7, out method consistently outperforms STPN [21] and Auto-loc [28] on all testing dataset. For instance, on the THUMOS14 dataset, when IoU threshold is 0.3, ours based on TSN features achieve a 37.3 mAP whereas Auto-Loc only achieves a 35.8 mAP. On the Acitivitynet 1.3, ours achieve a 19.0 mAP when IoU= 0.75, whereas STPN [21] only achieves a 16.9 mAP. Meanwhile, we achieve comparable performance with W-TALC [22] using the same I3D features. We visualize the detection result of a 2-phase setting on THUMOS'14 dataset in Figure 5. As shown in the figure, the proposed method not only detects most of action instances but also discover a temporal structure for each action instance.

5. Conclusion

In this paper, we investigate the problem of weakly supervised action detection (WSAD) in untrimmed videos and propose temporal structure mining (TSM) approach. Different from existing WSAD methods ignoring the temporal relation among segments, our TSM exploits the temporal structure in action instances. We model an action as a multiple-phase process and define temporal structure as the pattern of phase evolving. To effectively model videos containing multiple action instances, we design a recurrent phase evolving mechanism. We utilize phase filters to describe the confidence score of the presence of a specific action phase in a segment. Due to the lack of temporal annotation in training data, we treat the phase of a segment as a hidden variable which is determined by maximal circulant path discovery in the confidence score table. Extensive experiments conducted on three public datasets demonstrates the superiority of the proposed TSM in WSAD.

Acknowledgement: It is supported by start-up grants from University at Buffalo and a gift grant from Snap Inc.

References

[1] Hakan Bilen and Andrea Vedaldi. Weakly supervised deep detection networks. In *CVPR*, 2016.

[2] Piotr Bojanowski, Rémi Lajugie, Francis Bach, Ivan Laptev, Jean Ponce, Cordelia Schmid, and Josef Sivic. Weakly supervised action labeling in videos under ordering constraints. In *ECCV*, 2014.

[3] S Buch, V Escorcia, B Ghanem, L Fei-Fei, and JC Niebles. End-to-end, single-stream temporal action detection in untrimmed videos. In *BMVC*, 2017.

[4] Fabian Caba Heilbron, Victor Escorcia, Bernard Ghanem, and Juan Carlos Niebles. Activitynet: A large-scale video benchmark for human activity understanding. In *CVPR*, 2015.

[5] Joao Carreira and Andrew Zisserman. Quo vadis, action recognition? a new model and the kinetics dataset. In *CVPR*, pages 4724–4733, 2017.

[6] Chien-Yi Chang, De-An Huang, Yanan Sui, Li Fei-Fei, and Juan Carlos Niebles. D^3tw: Discriminative differentiable dynamic time warping for weakly supervised action alignment and segmentation. *CoRR*, abs/1901.02598, 2019.

[7] Yu-Wei Chao, Sudheendra Vijayanarasimhan, Bryan Seybold, David A Ross, Jia Deng, and Rahul Sukthankar. Rethinking the faster R-CNN architecture for temporal action localization. In *CVPR*, 2018.

[8] Xiyang Dai, Bharat Singh, Guyue Zhang, Larry S Davis, and Yan Qiu Chen. Temporal context network for activity localization in videos. In *ICCV*, 2017.

[9] Achal Dave, Olga Russakovsky, and Deva Ramanan. Predictivecorrective networks for action detection. In *CVPR*, 2017.

[10] Tran Du, Yuan Junsong, and David Forsyth. Video event detection: From subvolume localization to spatiotemporal path search. *IEEE Transactions on Pattern Analysis and Machine Intelligence*, 36(2):404–416, 2013.

[11] Adrien Gaidon, Zaid Harchaoui, and Cordelia Schmid. Actom sequence models for efficient action detection. In *CVPR 2011*, pages 3201–3208. IEEE, 2011.

[12] Yu Gang and Junsong Yuan. Fast action proposals for human action detection and search. In *CVPR*, 2015.

[13] Jiyang Gao, Zhenheng Yang, and Ram Nevatia. Cascaded boundary regression for temporal action detection. In *BMVC*, 2017.

[14] A Gorban, H Idrees, YG Jiang, A Roshan Zamir, I Laptev, M Shah, and R Sukthankar. Thumos challenge: Action recognition with a large number of classes, 2015.

[15] Fabian Caba Heilbron, Wayner Barrios, Victor Escorcia, and Bernard Ghanem. Scc: Semantic context cascade for efficient action detection. In *CVPR*, 2017.

[16] Rui Hou, Rahul Sukthankar, and Mubarak Shah. Real-time temporal action localization in untrimmed videos by subaction discovery. In *BMVC*, 2017.

[17] Will Kay, Joao Carreira, Karen Simonyan, Brian Zhang, Chloe Hillier, Sudheendra Vijayanarasimhan, Fabio Viola, Tim Green, Trevor Back, Paul Natsev, et al. The kinetics human action video dataset. *arXiv preprint arXiv:1705.06950*, 2017.

[18] Weixin Li and Nuno Vasconcelos. Recognizing activities by attribute dynamics. *NIPS*, 2013.

[19] Tianwei Lin, Xu Zhao, and Zheng Shou. Single shot temporal action detection. In *ACM on Multimedia*, 2017.

[20] Alberto Montes, Amaia Salvador, Santiago Pascual, and Xavier Giro-i Nieto. Temporal activity detection in untrimmed videos with recurrent neural networks. *arXiv preprint arXiv:1608.08128*, 2016.

[21] Phuc Nguyen, Ting Liu, Gautam Prasad, and Bohyung Han. Weakly supervised action localization by sparse temporal pooling network. In *CVPR*, 2018.

[22] Sujoy Paul, Sourya Roy, and Amit K Roy-Chowdhury. W-talc: Weakly-supervised temporal activity localization and classification. In *ECCV*, 2018.

[23] Colin Lea Michael D Flynn René and Vidal Austin Reiter Gregory D Hager. Temporal convolutional networks for action segmentation and detection. In *ICCV*, 2017.

[24] Alexander Richard, Hilde Kuehne, and Juergen Gall. Weakly supervised action learning with RNN based fine-to-coarse modeling. In *CVPR*, pages 1273–1282, 2017.

[25] Alexander Richard, Hilde Kuehne, Ahsan Iqbal, and Juergen Gall. Neuralnetwork-viterbi: A framework for weakly supervised video learning. In *ECCV*, 2018.

[26] Michael S Ryoo and Jake K Aggarwal. Semantic representation and recognition of continued and recursive human activities. *IJCV*, 82(1), 2009.

[27] Zheng Shou, Jonathan Chan, Alireza Zareian, Kazuyuki Miyazawa, and Shih-Fu Chang. Cdc: Convolutional-de-convolutional networks for precise temporal action localization in untrimmed videos. In *CVPR*, pages 1417–1426, 2017.

[28] Zheng Shou, Hang Gao, Lei Zhang, Kazuyuki Miyazawa, and Shih-Fu Chang. Autoloc: Weakly-supervised temporal action localization in untrimmed videos. In *ECCV*, pages 154–171, 2018.

[29] Zheng Shou, Dongang Wang, and Shih-Fu Chang. Temporal action localization in untrimmed videos via multi-stage cnns. In *CVPR*, 2016.

[30] Karen Simonyan and Andrew Zisserman. Two-stream convolutional networks for action recognition in videos. In *NIPS*, 2014.

[31] Krishna Kumar Singh and Yong Jae Lee. Hide-and-seek: Forcing a network to be meticulous for weakly-supervised object and action localization. In *ICCV*, 2017.

[32] Chen Sun and Ram Nevatia. Active: Activity concept transitions in video event classification. In *ICCV*, 2013.

[33] Chen Sun, Sanketh Shetty, Rahul Sukthankar, and Ram Nevatia. Temporal localization of fine-grained actions in videos by domain transfer from web images. In *ACM on Multimedia*, 2015.

[34] Kevin Tang, Li Fei-Fei, and Daphne Koller. Learning latent temporal structure for complex event detection. In *CVPR*, 2012.

[35] Du Tran, Lubomir Bourdev, Rob Fergus, Lorenzo Torresani, and Manohar Paluri. Learning spatiotemporal features with 3d convolutional networks. In *ICCV*, 2015.

[36] Du Tran and Junsong Yuan. Max-margin structured output regression for spatio-temporal action localization. In *NIPS*, 2012.

[37] Zhigang Tu, Hongyan Li, Dejun Zhang, Justin Dauwels, and Junsong Yuan. Action-stage emphasized spatio-temporal vlad for video action recognition. *IEEE Transactions on Image Processing*, 28(6):2799–2812, 2019.

[38] Zhigang Tu, Xie Wei, Qianqing Qin, Ronald Poppe, Remco C. Veltkamp, Baoxin Li, and Junsong Yuan. Multi-stream cnn: Learning representations based on human-related regions for action recognition. *Pattern Recognition*, 79:32–43, 2018.

[39] Limin Wang, Yu Qiao, and Xiaoou Tang. Mining motion atoms and phrases for complex action recognition. In *ICCV*, 2013.

[40] Limin Wang, Yuanjun Xiong, Dahua Lin, and Luc Van Gool. Untrimmednets for weakly supervised action recognition and detection. In *CVPR*, 2017.

[41] Limin Wang, Yuanjun Xiong, Zhe Wang, Yu Qiao, Dahua Lin, Xiaoou Tang, and Luc Van Gool. Temporal segment networks: Towards good practices for deep action recognition. In *ECCV*, 2016.

[42] Andreas Wedel, Thomas Pock, Christopher Zach, Horst Bischof, and Daniel Cremers. An improved algorithm for tv-l 1 optical flow. In *Statistical and geometrical approaches to visual motion analysis*. Springer, 2009.

[43] Huijuan Xu, Abir Das, and Kate Saenko. R-C3D: region convolutional 3D network for temporal activity detection. In *ICCV*, pages 5794–5803, 2017.

[44] Serena Yeung, Olga Russakovsky, Greg Mori, and Li Fei-Fei. End-to-end learning of action detection from frame glimpses in videos. In *CVPR*, 2016.

[45] Jun Yuan, Bingbing Ni, Xiaokang Yang, and Ashraf A Kassim. Temporal action localization with pyramid of score distribution features. In *CVPR*, 2016.

[46] Ze-Huan Yuan, Jonathan C Stroud, Tong Lu, and Jia Deng. Temporal action localization by structured maximal sums. In *CVPR*, 2017.

[47] Yue Zhao, Yuanjun Xiong, Limin Wang, Zhirong Wu, Xiaoou Tang, and Dahua Lin. Temporal action detection with structured segment networks. In *ICCV*, 2017.